Int J Thermophys (2008) 29:1–17
DOI 10.1007/s10765-007-0249-0

A Determination of the Ratio of the Zinc Freezing Point to the Tin Freezing Point by Noise Thermometry

J. R. Labenski · W. L. Tew · S. P. Benz · S. W. Nam · P. Dresselhaus

Published online: 12 September 2007

Abstract A Johnson-noise thermometer (JNT) has been used with a quantized voltage noise source (QVNS), as a calculable reference to determine the ratio of temperatures near the Zn freezing point to those near the Sn freezing point. The temperatures are derived in a series of separate measurements comparing the synthesized noise power from the QVNS with that of Johnson noise from a known resistance. The synthesized noise power is digitally programed to match the thermal noise powers at both temperatures and provides the principle means of scaling the temperatures. This produces a relatively flat spectrum for the ratio of spectral noise densities, which is close to unity in the low-frequency limit. The data are analyzed as relative spectral ratios over the 4.8 to 450 kHz range averaged over a 3.2 kHz bandwidth. A three-parameter model is used to account for differences in time constants that are inherently temperature dependent. A drift effect of approximately $-6\,\mu\mathrm{K}\cdot\mathrm{K}^{-1}$ per day is observed in the results, and an empirical correction is applied to yield a relative difference in temperature ratios of $-11.5 \pm 43\,\mu\mathrm{K}\cdot\mathrm{K}^{-1}$ with respect to the ratio of temperatures assigned on the International Temperature Scale of 1990 (ITS-90). When these noise thermometry results are combined with results from acoustic gas thermometry at temperatures near the Sn freezing point, a value of $T - T_{90} = 7 \pm 30\,\mathrm{mK}$ for the Zn freezing point is derived.

J. R. Labenski · W. L. Tew (✉)
Process Measurements Division, National Institute of Standards and Technology,
100 Bureau Drive, MS 8363, Gaithersburg, MD 20899, USA
e-mail: weston.tew@nist.gov

S. P. Benz · P. Dresselhaus
Quantum Electrical Metrology Division, National Institute of Standards and Technology,
Boulder, CO 80305, USA

S. W. Nam
Optoelectronics Division, National Institute of Standards and Technology, Boulder, CO 80305, USA

Keywords ITS-90 · Johnson noise · Josephson junction arrays · Noise thermometry · Power spectral density ratio · Pseudo noise · Temperature · Temperature measurement

1 Introduction

We report new Johnson-noise thermometry (JNT) measurements of the ratio of temperatures near the Zn freezing point, 693 K, to those near the Sn freezing point, 505 K, using a quantized voltage noise source (QVNS) [1], as a calculable reference noise source. The QVNS serves as a programmable noise source with a fixed-impedance matched to the spectral noise density of a thermal noise source. The thermal noise source is maintained at different times at one of these two temperatures, which are known on the International Temperature Scale of 1990 (ITS-90) [2] using a standard platinum resistance thermometer (SPRT). The end result is the difference between the temperature ratio as determined by noise thermometry and the ratio as defined on the ITS-90.

The spectral power density, S_R, of Johnson noise voltage fluctuations across a resistor R at a temperature T is given by the Nyquist formula

$$S_R = 4kTR, \tag{1}$$

where k is Boltzmann's constant. The spectral density S_J of the QVNS is produced by a pseudo-random-noise waveform using a harmonic series of tones. The amplitudes of the tones are equal while their relative phases are random so that their superposition on average generates a constant spectral density. The programmability of the QVNS and its inherent stability allows the spectral density to be matched to that of the Johnson noise from any RT combination [3].

1.1 Absolute Mode

The absolute temperature of the resistor can be found directly by taking the ratio of the noise spectra from two independent sources. In this "absolute" mode [4] the thermodynamic temperature is given by

$$T = \left\langle \frac{S_R}{S_J} \right\rangle \Bigg|_{f=0} \frac{S_{J\text{-calc}}}{4kR}, \tag{2}$$

where $\langle S_R/S_J \rangle$ is the average ratio of measured spectral densities from the resistor and QVNS, respectively, R is the measured resistance of the temperature probe, and $S_{J\text{-calc}}$ is the calculated spectral density of the QVNS reference waveform. The averaged spectral ratio is fitted with a three-parameter quadratic function in frequency, $a_2 f^2 + a_1 f + a_0$, where the offset term, $a_0 \cong 1$, is the value of the noise ratio spectrum in the low-frequency limit. The fitting accounts for the frequency dependence of the two transmission lines, as coupled to the source and input impedances [5]. Extrapolation of the spectral ratios to zero frequency allows for a larger measurement bandwidth

to be used than it would otherwise be possible by simply taking the average of the spectral density ratio over a limited low-frequency range.

1.2 Relative Mode

The "relative" temperature between two independent absolute temperature measurements can be determined by taking the ratio of the averaged power spectral ratios [6]. For two measurements at temperatures T_1 and T_2 and probe resistances R_1 and R_2, respectively, the relative thermodynamic temperature is given by the double ratio expression

$$T_2 = \left\langle \frac{S_{R2}}{S_{J2}} \right\rangle \left\langle \frac{S_{J1}}{S_{R1}} \right\rangle \Bigg|_{f=0} \frac{S_{J2\text{-calc}}}{S_{J1\text{-calc}}} \frac{R_1}{R_2} T_1. \tag{3}$$

The use of the relative mode has advantages in that most common systematic and frequency dependent effects from the transmission lines cancel in the double ratio. The remaining effects that do not cancel are from the temperature dependence of the materials used for the temperature probe at temperatures T_1 and T_2. The reference temperature T_1 may be any temperature that is known within a sufficient uncertainty. The temperatures reported here are derived according to Eq. 3.

2 Experimental

The JNT cross-correlation electronics consists of two independent differential-input, high-gain, amplifier channels, x and y, sampled by 14 bit, 50 M samples s^{-1} analog-to-digital converters. The raw data is processed by field programmable gate arrays (FPGAs) that implement a digital 200 kHz low-pass filter and down-sample to 2^{21} Samples s^{-1}. Fast-Fourier-transforms (FFTs) are computed for both channels and the corresponding auto-correlation spectra v_x^2 and v_y^2 are generated. A cross-correlated power spectrum, $S_c = v_x v_y^*$, between the two channels is likewise computed and recorded. The amplifier channels alternately measure the noise voltages from the two noise sources, temperature probe, and QVNS reference (i.e., the inputs are "chopped") for 100 s at a time to minimize the effects of amplifier drift, so that one full "chop" = 200 s of data. The noise measurements are paused for 43 s after every 10 chops, and the resistance of the temperature probe is measured.

The temperature probe contains resistance elements connected as a differential pair using wire-wound Pt–W alloy resistors (50 μm diameter), housed in alumina tubes, in a five-wire configuration [7]. The total resistance for the pair is $R(505\,\mathrm{K}) \approx 107\,\Omega$ and $R(693\,\mathrm{K}) \approx 113\,\Omega$ due to the $\sim 300\,\mu\Omega\,\Omega^{-1}\,K^{-1}$) temperature coefficient of the alloy. A pair of parallel, two-bore platinum-coated-quartz insulators, axially twisted by 90° at three locations along their length, and an external "fifth" wire ground are used to define parallel transmission lines within the probe length. The probe is housed in a 1.1 cm diameter, platinum-coated-quartz tube and inserted into a 41 cm deep thermowell within a three-zone vacuum furnace.

Table 1 Summary of absolute ratio data

Run	Date[a]	Group	Chops[b]	T_{90}[c] (K)	S_{T90}[d] (K)	ε[e] bin ($\mu K \cdot K^{-1}$)	S_{fit}[f] ($\mu K \cdot K^{-1}$)	ε[g] peak ($\mu K \cdot K^{-1}$)	S_{fit}[f] ($\mu K \cdot K^{-1}$)
1	9/13	Sn1	310	504.999	0.0002	4	69	3	67
2	9/14	Sn1	434	504.999	0.0007	75	70	73	70
3	9/17	Zn1	310	693.546	0.0005	48	74	87	74
4	9/18	Zn1	320	693.573	0.0016	−107	72	−45	72
5	9/19	Zn1	360	693.567	0.0024	17	70	29	71
6	9/20	Zn1	314	693.601	0.0029	32	71	−17	68
7	9/21	Zn2[h]	320	693.59	0.0026	109	81	−3	76
8	9/25	Zn2	682	693.532	0.0059	−13	68	−38	66
9	9/27	Zn2	169	693.518	0.0017	75	85	−42	81
10	9/28	Zn2	520	693.505	0.0049	7	72	−77	70
11	10/4	Sn2	701	505.004	0.0008	−145	61	−93	62
12	10/6	Sn2	1,150	505.019	0.0023	−161	59	−76	58

[a] Data taken September and October 2006

[b] Number of 100 s-long-noise samples per noise source measurement, 1 Chop = 200 s total

[c] Mean temperature of the Johnson noise probe

[d] Standard deviation of furnace temperature measurements

[e] $(T - T_{90})/T_{90}$ for the three-parameter fit using the full 3.2 kHz bandwidth around the QVNS tones

[f] Uncertainty in the offset parameter, a_0, from the least-squares fit

[g] $(T - T_{90})/T_{90}$ for the three-parameter fit using only the power in the QVNS tone

[h] Zn2 runs had 320 pF compensation capacitors on the QVNS input

The vacuum-furnace temperature is controlled using industrial platinum resistance thermometers (IPRTs) measured by direct current (DC) resistance bridges. Heating is done by low-voltage DC (15–30 V) bi-filar elements with a total power input to the furnace of less than 100 W. The temperature of the furnace is measured every 4 min by 25.5Ω, long-stem SPRTs calibrated at NIST [8] on the ITS-90 and installed in adjacent thermowells of the furnace. We checked the water triple-point (WTP) values between changes in furnace temperature or every 10–20 days of measurement, whichever comes first. Previous measurements with this system [7] were made using another thermal noise source, as a reference maintained at ∼312 K where the thermodynamic temperature is well known from acoustic thermometry [9]. That sub-system is not necessary for these experiments.

At 693 K, the furnace drifted by $\sim 0.5\,mK \cdot h^{-1}$, possibly due to drift in the industrial platinum resistance thermometers (IPRTs) used as sensors for the controllers. Even over the long duration runs such as #8 in Table 1 (∼40 h), the furnace drift produced a relatively small standard deviation, $S_{T90} \cong 5.8$ mK in T_{90} or $\sim 8.6\,\mu K \cdot K^{-1}$. Since the drift was predominately linear, the use of average values makes the results relatively unaffected by this drift. The furnace was stable to ±1 mK at 505 K. Similarly, we found the Pt–W alloy resistors to be highly stable and reproducible, with no indication of drift or hysteresis throughout a 6-month period of use.

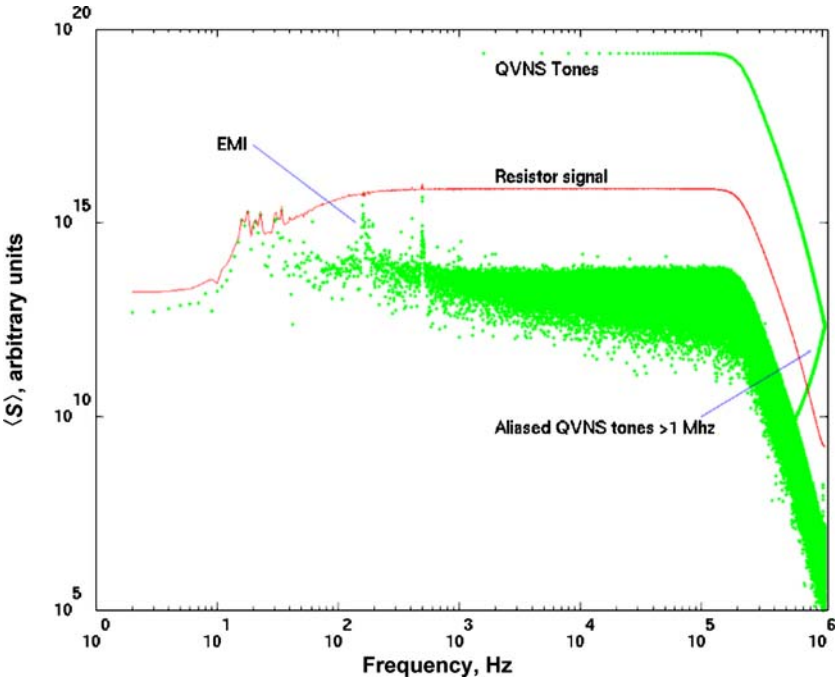

Fig. 1 Cross-correlated power spectrum from the QVNS and a 107.8 Ω resistor source at 505 K averaged over 43,400 s. The measured QVNS signal or pseudo-noise is shown as single-bin tones with fixed amplitudes $\sim 3.5 \times 10^5$ above the correlated noise floor

The QVNS uses dual arrays of 256 Josephson junctions maintained at 4.2 K in a liquid He Dewar. The pseudo-noise spectrum is synthesized by generating an odd harmonic series of equal-amplitude tones and random phases from 1.6 kHz up to 4 MHz in steps of 3.2 kHz. The amplitude of each harmonic is set so that the power over the 3.2 kHz bandwidth is equal to the power from the probe resistor over the same frequency range. In order to approximately match the impedance of the QVNS to that of the resistance probe, 51 Ω thin-film resistors were placed in series with each of the four-wire leads just after the Josephson junctions. The 4.2 K Johnson noise from these resistors submerged in liquid He is small in magnitude and uncorrelated between the two amplifiers, so it does not contribute to the correlated power spectrum from the QVNS.

Figure 1 shows the average of the spectral power density from the resistive and QVNS sources over a complete 24 h run. The noise floor of the system can be seen in the QVNS spectrum between the synthesized tones. Each tone is located entirely within a 1-Hz resolution bandwidth of the FFT. Aliased tones can be seen wrapping back from the Nyquist frequency of 2^{20} Hz but are attenuated by the 200 kHz 3 db 8-pole butterworth digital filter. Electromagnetic interference (EMI) can be seen in the low-frequency regions of the QVNS and resistor spectra, but those low frequencies are discarded in the spectral analysis. Higher frequency EMI is also discernible in the

QVNS spectrum, but these appear in only tens of 1 Hz bins and are just above the noise floor of the system, more than 50 dB below the power of the QVNS tones.

3 Results

We analyzed and combined 12 measurement runs totaling over 310 h, as summarized in Table 1. The "chops" column is the number of 200 s-long noise samples taken for both the temperature probe and the QVNS. Two runs at 505 K were taken during the first week of measurements. The furnace was then ramped up to 693 K where eight more runs were taken during the second and third weeks. The first four 693 K runs were slightly impedance mismatched, resulting in some frequency dependence from their transmission line *RC* coupling [5]. In the second set of four runs we "compensated" the frequency dependence of the transmission network from the Josephson junction array by placing 320 pF low-loss "NPO"-type capacitors across each of the four signal lines to the "5th-wire" ground. These capacitors were placed just before the input to the switch-card and resulted in a flatter frequency response in the absolute ratio spectra and the opposite curvature compared to the first set of Zn spectra (see trace "Zn2" in Fig. 2). As a check of the reproducibility, the furnace temperature was turned back down to 505 K and we took two more runs during the fourth week to complete the experiment. Our most ambitious run was the last 505 K run of 1,150 chops or ∼64 h of noise data. In all cases the noise power spectral densities were matched to better than 0.2% at low frequencies.

The runs were separated into four logical "groups," see Table 1, and combined as weighted-averages using the fraction of the number of chops for a single run to the total number of chops in the group. The first two runs at 505 K formed group "Sn1" and had similar spectral characteristics. The last two 505 K datasets, designated "Sn2," were also similar to each other. The 693 K data could be broken into two groups of four runs each, group "Zn1" which was not frequency compensated and group "Zn2" which was compensated. The absolute power spectral ratios of the four datasets are shown in Fig. 2. The change in the frequency roll-off of the Zn1 group spectrum compared to that of the Sn1 and Sn2 group ratios is primarily due to the increase in the temperature probe's resistance, $R(693\,\mathrm{K}) - R(505\,\mathrm{K}) \approx 5.5\ \Omega$. The Zn2 power spectrum demonstrates our ability to compensate for the mismatch in the time constants between the two noise sources using capacitors. All these grouped absolute spectra, however, exhibit some degree of higher-order frequency dependence, which cannot be fit using a quadratic function.

3.1 Absolute Ratios

The results of the absolute mode measurements are shown in Table 1, as the relative temperature difference, $\varepsilon = (T - T_{90})/T_{90}$. These results are derived from three-parameter fits of the noise power ratio spectra shown in Fig. 2, where T_{90} is the temperature measured by the SPRTs on the ITS-90. The fits were over a 4.8 to 446.4 kHz frequency range, excluding the first QVNS frequency tone centered at 1.6 kHz due to the influence of low-frequency EMI which becomes appreciable below 500 Hz. The

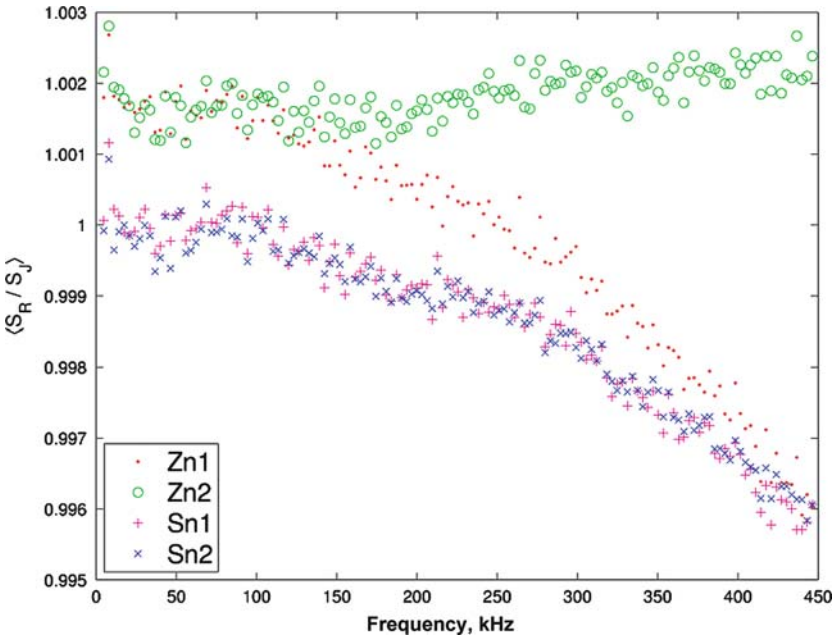

Fig. 2 Absolute power spectrum ratios of the Sn and Zn datasets. Only the Zn2 dataset is capacitively compensated to flatten the spectrum ratio across the frequency band

highest frequency was limited to <450 kHz to avoid higher-order frequency (i.e., f^n, $n > 2$) terms in the fit. The zero-frequency intercept a_0 of each fit is related to the relative temperature difference ε by $a_0 = a_{90}(1 + \varepsilon) = a_{90}T/T_{90}$ for each absolute ratio dataset, where $a_{90} = 4\,kT_{90}R/S_{\text{J-calc}} \cong 1$. The relative statistical uncertainty in ε, shown in the column s_{fit}, is identical to the uncertainty of a_0 obtained from the covariance matrix of the least squares fit.

The ratios of the resistor to QVNS power spectra were performed in two ways. The "re-binned" results in Table 1 average the noise source data by taking the ratio of the power spectrum of the resistor to the QVNS over 3.2 kHz bandwidths centered on the QVNS tones. The "peak" results also re-bin the resistor data every 3.2 kHz, but use only the 1 Hz wide peak of the QVNS tone for the total power in the 3.2 kHz bandwidth. Figure 3 shows the results from Table 1 along with the results from a two-parameter fit, $a_2 f^2 + a_0$ for reference. The two-parameter fit ignores contributions to the frequency dependence from any lossy-dielectrics in the transmission lines [5]. The root-mean-square (rms) values for the T-statistic of the linear term of the three-parameter fit vary between data groups: 0.2 rms for Sn1; 0.6 rms for Sn2; 0.4 rms for Zn1; and 1.3 rms for Zn2; in the peak results. So inclusion of the linear term is only necessary on purely statistical grounds for the Zn2 and Sn2 data groups. For both two- and three-parameter fits, however, Fig. 3 suggests a gradual time dependence to the relative differences ε during the progression of runs over the four-week experimental sequence.

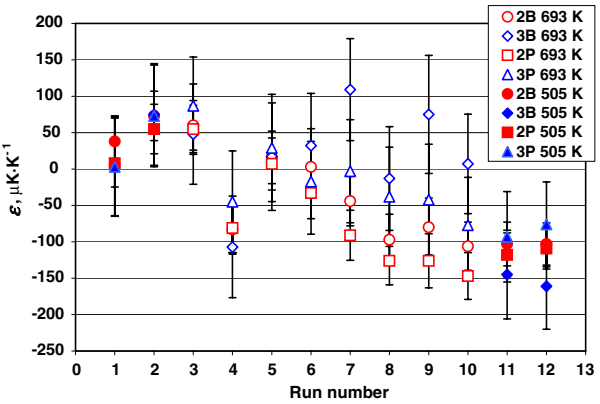

Fig. 3 Results of $\varepsilon = (T - T_{90})/T_{90}$ from Table 1 with error bars from the fit statistics of the offset parameter, a_0. Both two- and three-parameter fits are shown for power spectral ratios that use 3.2 kHz frequency bandwidth for both the temperature probe and the QVNS and ratios using only the QVNS "peak" tones

We combined the ratios for the grouped runs into a weighted average, weighting each run by the number of chops, and then fit a three-parameter polynomial function to the re-binned ratios to obtain: $\varepsilon_{\mathrm{Sn1}} = (45 \pm 64)\,\mu\mathrm{K{\cdot}K^{-1}}$, $\varepsilon_{\mathrm{Sn2}} = -(155 \pm 56)\,\mu\mathrm{K{\cdot}K^{-1}}$, $\varepsilon_{\mathrm{Zn1}} = -(2 \pm 62)\,\mu\mathrm{K{\cdot}K^{-1}}$, $\varepsilon_{\mathrm{Zn2}} = (25 \pm 66)\,\mu\mathrm{K{\cdot}K^{-1}}$, where the uncertainty shown is only the statistical error in ε. If only the QVNS peaks are used to create the spectral ratio, the results become: $\varepsilon_{\mathrm{Sn1}} = (44 \pm 64)\,\mu\mathrm{K{\cdot}K^{-1}}$, $\varepsilon_{\mathrm{Sn2}} = -(82 \pm 57)\,\mu\mathrm{K{\cdot}K^{-1}}$, $\varepsilon_{\mathrm{Zn1}} = (14 \pm 63)\,\mu\mathrm{K{\cdot}K^{-1}}$, $\varepsilon_{\mathrm{Zn2}} = -(44 \pm 64)\,\mu\mathrm{K{\cdot}K^{-1}}$. In both cases the results from the two Sn data groups differ by ≥ 2 standard uncertainties suggesting a systematic shift in the absolute spectra between the Sn1 and Sn2 data groups over the intervening 3 weeks.

3.2 Relative Ratios

The relative ratio spectra of the four data groups are shown in Fig. 4. The simple three-parameter quadratic function fits these spectra generally better than the absolute ratio spectra (Fig. 2) due to cancellation of common higher-order frequency dependence and QVNS tone-amplitude distortion.

Figure 5 shows the residuals of the three-parameter fits of both absolute and relative spectral ratios for the two data groups Sn1 and Zn1. The higher-order frequency components are evident in the absolute ratio residuals. These higher-order features are significantly diminished in the residuals of the Zn1/Sn1 relative ratio spectrum. The standard deviations of the fit parameters are reduced by $\sim 50\%$ in the relative ratio spectra compared to the absolute ratios, whereas random statistics alone would predict an increase by a factor $\sim 2^{1/2}$.

Table 2 shows the results from the relative ratio spectra, presented as the relative difference in the ratio of the noise temperatures at 693 and 505 K from the ITS-90

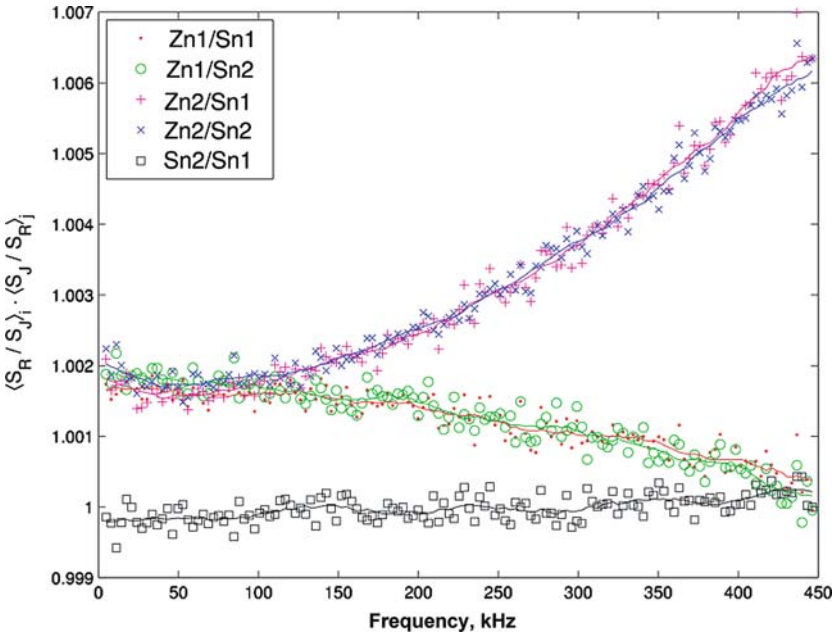

Fig. 4 Power spectral ratio of the four grouped datasets from Table 1 as well as the ratio of two Sn groups. Both Sn data as well as Zn1 are not capacitively compensated so that their spectral ratio shows the change in the frequency response of the temperature noise probe between the two temperatures

Table 2 Summary of averaged relative-ratio data

Run[a]	$\varepsilon_{Zn} - \varepsilon_{Sn}$[a] bin ($\mu K \cdot K^{-1}$)	S_{fit}[b] ($\mu K \cdot K^{-1}$)	$\varepsilon_{Zn} - \varepsilon_{Sn}$[a] peak ($\mu K \cdot K^{-1}$)	S_{fit}[b] ($\mu K \cdot K^{-1}$)
Zn1/Sn1	−48	45	−31	43
Zn2/Sn1	−18	47	−86	44
Zn1/Sn2	152	43	95	42
Zn2/Sn2	182	42	41	38

[a] Normalized relative temperature ratio difference from ITS-90 using three-parameter fit

[b] Uncertainty in the offset parameter, a_0, from the least-squares fit

temperature ratio, or

$$\varepsilon_{Zn} - \varepsilon_{Sn} \cong \frac{T_{Zn}/T_{Sn} - T_{Zn-90}/T_{Sn-90}}{T_{Zn-90}/T_{Sn-90}}, \tag{4}$$

where the approximation is valid to order ε^2. As in the case of the absolute ratio spectra, we have analyzed the relative data using both ratios re-binned over the 3.2 kHz frequency bandwidth for both noise sources (i.e.,"bin") and using only the "peak" of the single-frequency tone from the QVNS. Figure 6 shows the results in Table 2 for the three-parameter fits, as well as for two-parameter fits that had been previously used for each of the four grouped data combinations.

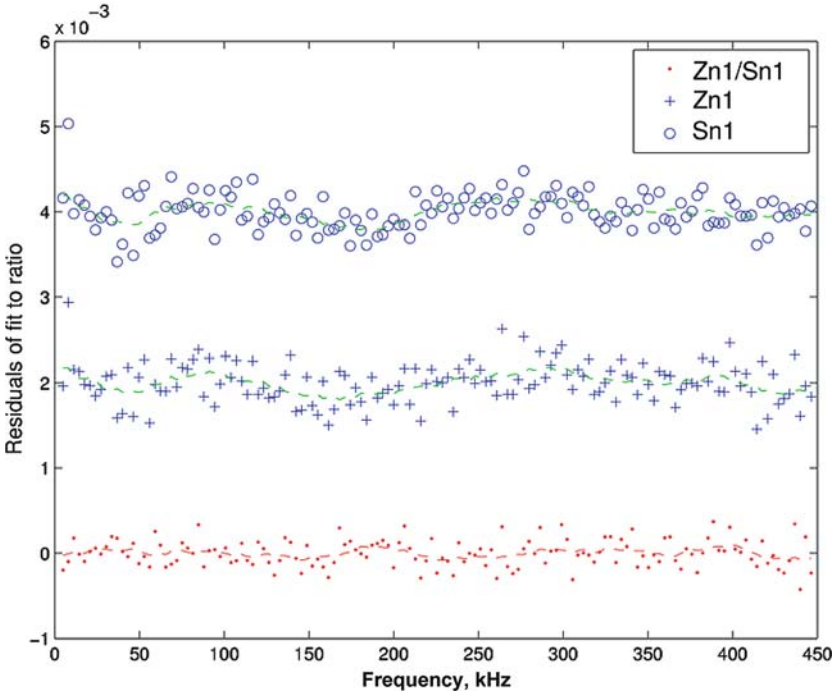

Fig. 5 Residuals to the three-parameter fits to the averaged Zn1, Sn1, and the double ratio between Zn1/Sn1 datasets. A 10 point run-average is shown for each curve to draw attention to the higher-order frequency dependence in the Zn1 and Sn1 residuals that is mostly removed in the double ratio. The Zn1 and Sn1 residuals are shifted upwards for clarity

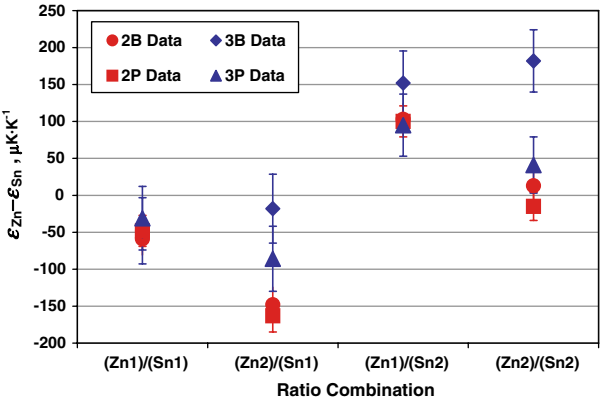

Fig. 6 Results of $\varepsilon_{Zn} - \varepsilon_{Sn}$ from Table 2 with error bars from the fit statistics of the offset parameter, a_0. Both two- and three-parameter fits are shown for power spectral ratios that use 3.2 kHz frequency bandwidth for both the temperature probe and the QVNS and ratios using only the QVNS "peak" tone

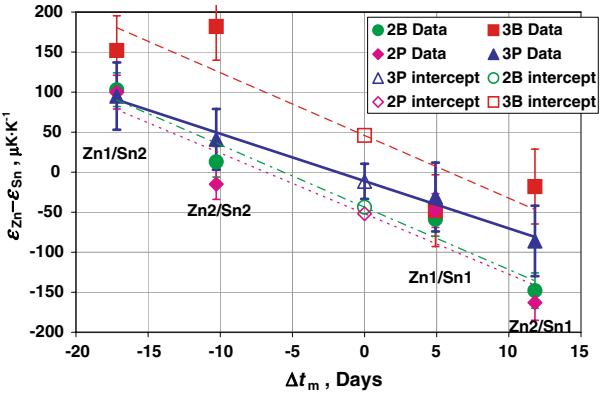

Fig. 7 Results for $\varepsilon_{\mathrm{Zn}} - \varepsilon_{\mathrm{Sn}}$ for the four analysis variations for the four data group combinations as a function of the time difference Δt between the Zni and Snj measurements

4 Discussion

In the previous section the data are analyzed in four different ways which are the product of: two ways of assigning QVNS averages for each 3.2 kHz bandwidth; and two spectral models having either two- or three-parameter fits. For the purposes of this discussion, we use the following notation: "2B," for a two-parameter fit of QVNS averages using all the data within the 3.2 kHz *bandwidth*; "3B," for a three-parameter fit of the same QVNS averages; "2P," for a two-parameter fit of QVNS averages using just the tone *peak* value for the entire 3.2 kHz bandwidth; and "3P," for a three-parameter fit of the same peak-value QVNS averages. Comparison of these different analysis methods allows some estimation of possible systematic effects. For reasons argued below, we use the 3P method for determining a final value of the measured temperature.

In addition to the four analysis methods, the four independent data groups (Sn1, Sn2, Zn1, and Zn2) are combined to form the four ratio permutations: Zn1/Sn1, Zn1/Sn2, Zn2/Sn1, and Zn2/Sn2. All of these permutations will be used for the determination. The choice is then in how to best average the four permutations.

4.1 Time Dependence

The 693 K absolute ratio data, groups Zn1 and Zn2, suggest the presence of a downward trend in ε over time, except for the #4 run (see Fig. 3). If the 505 K data are taken into account, as well, the $\sim 150\,\mu\mathrm{K}\cdot\mathrm{K}^{-1}$ downward shift over 4 weeks is roughly consistent with the apparent drift in the 693 K data except for the 3B analysis.

Another way to characterize this shift over time is by taking relative ratios of the 505 K data (i.e., Sn2/Sn1). The resultant double ratio spectrum should be flat if all time constants in the system are unchanged, and ε for these ratios should be zero to within

statistical uncertainty. This was found to be the case for proximal ratio combinations between the two Sn1 measurement runs (runs 1 and 2) as well as the two Sn2 runs (runs 11 and 12) where typically $\varepsilon \leq (50 \pm 50)\,\mu\mathrm{K{\cdot}K^{-1}}$. Ratios between the fourth and first week 505 K groups Sn2 and Sn1, however, do show a significant apparent offset in the range $\varepsilon \approx 165\,\mu\mathrm{K{\cdot}K^{-1}}$ for the 3P analysis. This offset is accompanied by a linear trend of $\sim 0.8\,\mu\mathrm{K{\cdot}K^{-1}\,kHz^{-1}}$ in the ratio spectrum. This effect can be seen in Fig. 4 as the ratio of the groups Sn2 to Sn1. The offset is consistent in magnitude and sign with the effects found comparing the Zni/Snj relative ratio data between the two Sn groups (i.e., $i \neq j$). Given that the mean measurement times for the Sn1 and Sn2 groups were separated by ∼22 days, the change in ε implies systematic drift rate of $\sim -7.5\,\mu\mathrm{K{\cdot}K^{-1}\,day^{-1}}$.

In order to compensate for the time dependence of the data, we introduce a relative time parameter Δt_{m}, which is the difference between the mean measurement times of the 693 K data and the 505 K data for a given ratio permutation. Figure 7 shows the relative ratio results as plotted against Δt_{m}, where all four analysis methods reveal a negative drift. The drift rates range from $-(5.9 \text{ to } 7.9)\,\mu\mathrm{K{\cdot}K^{-1}\,day^{-1}}$. We assume that results interpolated to $\Delta t_{\mathrm{m}} = 0$ will be corrected for the effects of the drift. This is equivalent to assuming that the drift rate is a constant, independent of both time and temperature. Since the drift is small, this assumption is probably valid unless the drift is associated with the temperature probe, in which case temperature dependence would be expected. Since chopping of the inputs cancels the effects of drift in the amplifiers, the drift is apparently manifest in one or both of the noise sources or their respective transmission-line networks.

4.2 Calculation of the Temperature Ratio and $\varepsilon_{\mathrm{Zn}}$

As shown in Fig. 7, the four analysis methods yield different values for the intercept parameter which represents $\varepsilon_{\mathrm{Zn}} - \varepsilon_{\mathrm{Sn}}$ at $\Delta t_{\mathrm{m}} = 0$. The linear regression results yield the following standard errors (of the fits) for the four analysis methods: 2B, $26.4\,\mu\mathrm{K{\cdot}K^{-1}}$; 3B, $62.4\,\mu\mathrm{K{\cdot}K^{-1}}$; 2P, $46.4\,\mu\mathrm{K{\cdot}K^{-1}}$; and 3P, $10.1\,\mu\mathrm{K{\cdot}K^{-1}}$. These fit statistics indicate the lower dispersion is found in the 3P analysis, which is also true even if no drift correction is applied and a simple mean or weighted mean is used to characterize the four distributions. The 3P is superior to the 2B and 3B analyses mainly due to the sensitivity of the 2B and 3B analyses to anomalous low frequency scatter in the re-binned ratio spectra below ∼40 kHz. The 2B fit is less sensitive to this scatter than is the 3B fit, but the effect is largely absent in the peak-analysis method. The 3P is superior to the 2P due to a small linear frequency dependence that is present in at least half of the data and most likely associated with dielectric loss.

The intercept parameter $\varepsilon_{\mathrm{Zn}} - \varepsilon_{\mathrm{Sn}}(\Delta t_{\mathrm{m}} = 0)$ for a weighted fit of the 3P analysis data yields $-11.5\,\mu\mathrm{K{\cdot}K^{-1}}$. An unweighted fit yields $-11.1\,\mu\mathrm{K{\cdot}K^{-1}}$, with practically the same drift rate of $-5.9\,\mu\mathrm{K{\cdot}K^{-1}\,day^{-1}}$. In order to obtain $\varepsilon_{\mathrm{Zn}}$ alone, we combined our result with the result of Strouse et al. [9] who determined $\varepsilon_{\mathrm{Sn}} = 21.2\,\mu\mathrm{K{\cdot}K^{-1}}$ via acoustic gas thermometry. The net result is then $\varepsilon_{\mathrm{Zn}} = 9.7\,\mu\mathrm{K{\cdot}K^{-1}}$ or $T_{\mathrm{Zn}} - T_{\mathrm{Zn\text{-}90}} = 6.7\,\mathrm{mK}$, as shown at the bottom section of Table 3.

Table 3 Uncertainty budget and result summary

Noise temperature uncertainties		$u(T)/T$ (μK · K^{-1})	$u(T)$ (mK)
Statistics (Standard Deviation)		30	20.8
Spectral model		9	6.2
EMI		26	17.9
Non-linearity		2	1.4
Time dependence		12	8.2
QVNS reference ratio		3	2.1
Resistance ratio		2	1.4
RSS		43	29.5
ITS-90 uncertainties			
505 K		5	2.6
693 K		7	5.0
Final results	ε(μK · K^{-1})		
$\varepsilon_{Zn} - \varepsilon_{Sn}$	−11.5	43	
Ref. T correction: ε_{Sn} [9]	21.2	6	4.1
ε_{Zn}	9.7	44	

4.3 Additional Systematic Checks

After the experiment was completed, we disassembled the high-temperature probe and measured the pair capacitance and loss tangent, tan δ, of both quartz insulators at 505 and 693 K. At 505 K, we found that the quartz exhibited low loss both at direct current (DC) and for frequencies up to 1 MHz with shunt resistance $\geq$1 G Ω and tan $\delta \leq 0.001$. At 693 K the DC shunt resistance was somewhat lower and more variable, generally in the range of 60–120 M Ω. The loss tangent was also somewhat variable over time, ranging between 2×10^{-2} and 8×10^{-3} for $f \geq 5$ kHz over a 6-week test period under normal atmospheric conditions. A low-frequency loss peak was also observed centered at ∼200 Hz with a peak value that varied between 3.5×10^{-2} and 1.6×10^{-2} over that same test period. The pair capacitance of the quartz at 5 kHz varied between 15 and 16 pF during the test. Some of these changes may have been due to adsorption effects, as similar magnitude changes could be observed by pumping out the test probe volume.

Given the predominately linear 505 K double ratio spectrum, a possible cause for the change in those spectra is a drift in a dielectric loss tangent from capacitance, somewhere in transmission lines. When expressed as a linear time constant τ, the linear coefficient from the Sn2/Sn1 relative ratio spectrum of $a_1 = 0.7 \times 10^{-6}$ kHz^{-1} implies $\tau \approx 1 \times 10^{-10}$ s. A model of the transmission line from source to preamplifier input [5] shows that a difference in the dielectric loss between the two inputs "1" and "2" gives rise to a linear frequency dependence of $2(C_2 R_2 \tan\delta_2 - C_1 R_1 \tan\delta_1)$ Ω, in the ratio spectrum where C_i is only that section of shunt capacitance, which exhibits the loss of magnitude $\tan\delta_i$. In practice, a double ratio spectrum such as the Sn2/Sn1 case

would only be sensitive to changes in the product $CR\tan\delta$ for either input. With that in mind, it is possible to produce the observed linear ratio spectrum effect by any change $2\Delta(CR\tan\delta) \approx 1 \times 10^{-10}$ s. When coupled to a 50 Ω termination, this means: 200 pF and $\Delta\tan\delta \approx 5 \times 10^{-3}$; or 20 pF and $\Delta\tan\delta \approx 5 \times 10^{-2}$; or 2 pF and $\Delta\tan\delta \approx 0.5$. However, this would only account for the change in the linear trend of the Sn2/Sn1 spectrum. In order to account for the accompanying offset drift, it is necessary to have a relatively large change (e.g., $\Delta\tan\delta \sim 1$ for 200 pF) in a low-frequency loss peak. But in that case the change must have the opposite sign to the change associated with the frequency-independent part of $\tan\delta$. Since we have not observed any changes in the insulators used in the experiment of this magnitude or complexity, the source of the drift is presently unexplained.

4.4 Uncertainties

The estimated standard uncertainties are summarized in Table 3. The individual components are considered uncorrelated and added in quadrature as a root-sum-square (RSS). The total RSS uncertainty in the temperature ratio T_{Zn}/T_{Sn} alone is $43\,\mu K{\cdot}K^{-1}$ and that of $\varepsilon_{Zn} - \varepsilon_{Sn}(\Delta t_m = 0)$ is also $43\,\mu K{\cdot}K^{-1}$ with respect to ITS-90 temperatures. When the result is corrected for the known value of ε_{Sn} [9], the uncertainty in ε_{Zn} is then $44\mu K{\cdot}K^{-1}$.

4.4.1 Statistics

A weighted linear regression fit of the four 3P ratios yields a standard error in the intercept of $22\,\mu K{\cdot}K^{-1}$, but this estimate underestimates the actual statistical uncertainty due to correlations in the ratio permutations which reduce the effective degrees of freedom in the fit. In order to obtain an accurate statistical uncertainty, we developed a simplified statistical model of four independent spectral power measurements, at two separate temperatures, subject to a linear drift. With model data based on the measured spectral ratio data, we obtain a statistical uncertainty of $30\,\mu K{\cdot}K^{-1}$ for $\varepsilon_{Zn} - \varepsilon_{Sn}(\Delta t_m = 0)$.

4.4.2 Spectral Model

There is uncertainty in the choice of the spectral model used to derive the low-frequency behavior of the ratio spectra. This arises from a certain degree of statistical ambiguity between the three-parameter fits and other possible models. While the 3P model is physically motivated, it is also possible that some additional mechanisms can introduce more complex behavior, as we have seen in the absolute spectra. Higher-order frequency dependence introduces errors, however, only to the extent that the extrapolation to $f = 0$ is affected. We estimate a type-B uncertainty for the spectral model by comparing the average 3P results with those derived from a simple mean of the frequencies below 50 kHz, which differ by $\sim 15\,\mu K{\cdot}K^{-1}$. This difference is well within statistical bounds, so we assign a rectangular distribution of $30\,\mu K{\cdot}K^{-1}$ full

width to account for any remaining unresolved effect, yielding a standard uncertainty component of $9\,\mu\mathrm{K}\cdot\mathrm{K}^{-1}$.

4.4.3 EMI

This type-B component accounts for all effects of interference in the data, both periodic, and broad (e.g., "white" noise) sources. These interferences can be coupled into the system as correlated stray signals either magnetically or through the ground as a result of imperfect common mode rejection (CMR). While large periodic interference is normally detectable in the raw 1 Hz-resolved power spectra, other types are not easily detected in any direct way. In this case, we utilize the comparison between the 3P and 3B results as an estimate for how large such effects might be in the QVNS probe. This comparison yields a difference of $57\,\mu\mathrm{K}\cdot\mathrm{K}^{-1}$ for the time-corrected results, which again is not statistically significant considering the higher uncertainty associated with the 3B data analysis. For uncertainty due to EMI in the QVNS output, we assign a rectangular distribution of full width $57\,\mu\mathrm{K}\cdot\mathrm{K}^{-1}$ and standard uncertainty $\sigma_{\mathrm{EMI\text{-}Q}} = 16\,\mu\mathrm{K}\cdot\mathrm{K}^{-1}$. In addition, we estimate an independent contribution of uncertainty from EMI in the temperature probe of $\sigma_{\mathrm{EMI\text{-}T}} = 20\,\mu\mathrm{K}\cdot\mathrm{K}^{-1}$ from our earlier analysis [7]. The combined uncertainty for EMI is then $\sigma_{\mathrm{EMI}} = (\sigma^2_{\mathrm{EMI\text{-}T}} + \sigma^2_{\mathrm{EMI\text{-}Q}})^{1/2} = 26\,\mu\mathrm{K}\cdot\mathrm{K}^{-1}$.

4.4.4 Time Dependence

The empirical correction of the time dependence of the data assumes a drift proportional to the absolute spectral ratio and linear in time. Possible deviations from these assumptions result in some additional uncertainty beyond the statistics associated with the correction model itself. If no drift correction is applied to the data, a reasonable statistic for comparison is the weighted mean, which is $\varepsilon_{\mathrm{Zn}} - \varepsilon_{\mathrm{Sn}} = +9\,\mu\mathrm{K}\cdot\mathrm{K}^{-1}$ for the 3P ratio distribution. This differs from our drift-corrected value by $20.5\,\mu\mathrm{K}\cdot\mathrm{K}^{-1}$, which again is not a significant difference. In this case, we assign the full width of a rectangular distribution to account for the uncertainty of the drift correction of twice this difference or $41\,\mu\mathrm{K}\cdot\mathrm{K}^{-1}$, yielding a standard uncertainty component of $12\,\mu\mathrm{K}\cdot\mathrm{K}^{-1}$.

4.4.5 Other Noise-related Uncertainties

The uncertainty budget of Table 3 contains several additional small contributions. Our estimated uncertainty for non-linearity is $2\,\mu\mathrm{K}\cdot\mathrm{K}^{-1}$ based on an earlier estimate [7]. We have neglected small corrections accounting for the finite resistance of gate resistors in parallel with the preamplifier input ($R_{\mathrm{g}} = 20\ \mathrm{M}\,\Omega$) [7], since these effects are of magnitude $\sim(R(693\,\mathrm{K}) - R(505\,\mathrm{K}))/R_{\mathrm{g}} < 1\,\mu\mathrm{K}\cdot\mathrm{K}^{-1}$ and are negligible. The uncertainty associated with the QVNS ratio of spectral densities refers to the relative waveform accuracy as generated at the output. This includes contributions from quantization errors, harmonic distortion, frequency stability, and input–output coupling [10]. The RSS uncertainty component is $\cong 3\,\mu\mathrm{K}\cdot\mathrm{K}^{-1}$.

4.4.6 ITS-90 Thermometry

The uncertainties associated with ITS-90 temperatures are shown in the second section of Table 3. These include contributions from measurement statistics, calibration, stability, temperature non-uniformity, and resistance ratios. During the 4 weeks of the experiment, only one SPRT was available for use, serial number 1422. However, this SPRT was used with other calibrated SPRTs in the same vacuum furnace both before and after these measurements. Those measurements showed agreement between the indicated T_{90} temperatures at both 505 and 693 K within the standard uncertainty components for thermal uniformity of 2 and 3 mK, respectively. The maximum observed change in the SPRTs WTP value was 0.34 mK during a 2-month period including the 4 weeks of the experiment. In addition, SPRT 1422 was re-calibrated at the Zn FP in December of 2006 and compared with the original November 2005 calibration. The difference was 1.1 mK, which again was within the uncertainty allowance for SPRT stability.

5 Conclusions

The ratio of temperatures near the Zn freezing point to those near the Sn freezing point have been determined via noise thermometry using a QVNS reference. We find $T_{Zn}/T_{Sn} = 1.37141 \pm 0.00006$. When expressed as a relative difference with respect to ITS-90 temperatures, the result is $\varepsilon_{\mathrm{Zn}} - \varepsilon_{\mathrm{Sn}} = -11.5 \pm 43\,\mu\mathrm{K{\cdot}K^{-1}}$. A drift rate of $-(6 \pm 2)\,\mu\mathrm{K{\cdot}K^{-1}\,day^{-1}}$ is observed in the data, and a relative time correction model is applied. When combined with results from acoustic gas thermometry at temperatures near the Sn freezing point, we obtain a value of $T - T_{90} = 7 \pm 30$ mK for the Zn freezing point. This result is well within one combined standard uncertainty from our earlier JNT result [7] at this temperature of $T - T_{90} = -14 \pm 24$ mK using only resistance-based scaling methods but with considerably more data. Further work is underway to: uncover the source of the time dependence; replicate these results using variations of the QVNS and alternative temperature probes; and perform similar determinations at higher temperatures.

Acknowledgments The authors wish to acknowledge the innovative design work and conceptual foundations contributed by John Martinis, while formerly at NIST. D. Rod White of the New Zealand Measurements Standards Laboratory, Industrial Research, Ltd. provided important design and theoretical contributions. Dean Ripple of the NIST Process Measurements Division provided many helpful suggestions and comments. We also thank Greg Strouse and Dennis Minor of the Process Measurements Division for providing the ITS-90 calibrations.

References

1. S.P. Benz, J.M. Martinis, P.D. Dresselhaus, S.W. Nam, IEEE Trans. Instrum. Meas. **52**, 545 (2003)
2. H. Preston-Thomas, Metrologia **27**, 3 (1990); **27**, 107 (1990)
3. S.P. Benz, J.M. Martinis, S.W. Nam, W.L. Tew, D.R. White, in *Proc. TEMPMEKO 2001*, ed. by B. Fellmuth, J. Seidel, G. Scholz (VDE Verlag, Berlin, 2002), pp. 37–44
4. S. Nam, S. Benz, P. Dresselhaus, W.L. Tew, D.R. White, J.M. Martinis, IEEE Trans. Instrum. Meas. **52**, 550 (2003)

5. J.R. Labenski, W.L. Tew, S.W. Nam, S.P. Benz, P.D. Dresselhaus, C.J. Burroughs, IEEE Trans. Instrum. Meas. **56**, 481 (2007)
6. S.W. Nam, S.P. Benz, J.M. Martinis, P. Dresselhaus, W.L. Tew, D.R. White, in *Temperature: Its Measurement and Control in Science and Industry*, vol. VII, ed. by D.C. Ripple (AIP, Melville, New York, 2003), pp. 37–42
7. W.L. Tew, J.R. Labenski, S.W. Nam, S. P. Benz, P.D. Dresselhaus, C.J. Burroughs, Int. J. Thermophys. **28**, 629 (2007)
8. B.W. Mangum, G.T. Furukawa, *NIST Tech. Note 1265* (Nat. Inst. Stds. Technol., Gaithersburg, Maryland, 1990)
9. G.F. Strouse, D.R. Defibaugh, M.R. Moldover, D.C. Ripple, in *Temperature: Its Measurement and Control in Science and Industry*, vol. VII, ed. by D.C. Ripple (AIP, Melville, New York, 2003), pp. 31–36
10. S.W. Nam, S.P. Benz, P. Dresselhaus, C.J. Burroughs, W.L. Tew, D.R. White, J.M. Martinis, IEEE Trans. Instrum. Meas. **54**, 653 (2005)